Closed-loop control of a spatially developing free shear flow around a steady state

Diemer Anda-Ondo, Christophe Collewet, Johan Carlier

Closed-loop control of a spatially developing free shear flow around a steady state ⋆

D. Anda-Ondo * **J. Carlier** *,** **C. Collewet** *,**

* *Irstea, UR Opaale, F-35044 Rennes Cedex, France*
** *Inria, Fluminance Project, F-35042 Rennes Cedex, France*

Abstract:
This paper provides preliminary results on the closed-loop control of a spatially developing mixing-layer induced by two parallel incident streams with different velocities. The goal of the control law was to stabilize the flow around a desired state (known to reduce mixing). The way to achieve this flow control consists of linearizing the Navier-Stokes equations about the desired state, spatially discretizing the resulting linear system and determining the feedback gain according to an optimal control law. Actuations were located in the input boundary of the system. State of the flow was assumed to be reconstructed from image sensors. The control law has been validated on a realistic non-linear system (Navier-Stokes solver). More precisely, these simulation results have shown that perturbations can be efficiently rejected.

Keywords: Control of fluid flows and fluids-structures interactions; Output feedback control (linear case); Time-invariant systems.

1. INTRODUCTION

Entrainment and mixing processes in the turbulent layer between two adjacent fluids are commonly involved in industrial applications. In the case of a spatially developing plane shear layer, induced by two parallel incident streams with velocity differences, the flow is very sensitive to upstream boundary conditions. Flow control by acting on those upstream conditions is therefore a promising way to enhance or reduce mixing due to turbulence (for example: mixing increase in chemical industry; mixing reduction in food industry; energy consumption and noise reduction in air, road and train transportations).

Many studies showed periodic excitations act significantly on the mixing layer development. Open-loop control was achieved in Oster et al. (1978), Inoue (1992) and Zhou and Wygnanski (2001) using predetermined periodic excitations to study the vortex interactions and their effects on the growth of the mixing layer. Closed-loop control of the mixing layer was recently investigated in Kaul (2013), Kaul (2014) and Parezanović et al. (2015). In Kaul (2013) and Kaul (2014), a temporally developing mixing layer was used to make it easier to design a control law optimizing the thickness of the mixing layer (this control law being applied on a spatially developing mixing layer next). In Parezanović et al. (2015), turbulence in the mixing layer was increased using optimal frequency actuation deduced online (rather than offline as in previous studies using open-loop control) from different closed-loop methods (extremum-seeking adaptive control, POD mode feedback control, machine learning control).

⋆ We are grateful to the Brittany Regional Council of France for their financial support.

In the present study, we have developed closed-loop control to stabilize the mixing-layer about a steady desired state (as a first step in the way to cope with an unsteady desired state corresponding to a particular space-time organization of the flow knowing the benefits for industrial applications). The way to achieve flow control consists of linearizing the Navier-Stokes equations about the desired state, spatially discretizing the resulting linear system and determining the feedback gain according to an optimal control law. Actuations were located in the input boundary of the system. State of the flow was assumed to be reconstructed from image sensors. We called on a classical control scheme from control theory, i.e. state feedback by Linear-Quadratic Regulator (LQR), in accordance with Kim and Bewley (2007) and Brunton and Noack (2015), about linear control efficiency applied on non-linear turbulence dynamics.

The main contribution of this paper is to show that the mixing layer can be stabilized around a steady state from a linear control law based on a linearization around this desired state, even with slow disturbances in the incoming flow. The paper is structured as follows. Section 2 gives a brief description of the fluid flow. Section 3 is devoted to flow modeling and the closed-loop control design. Section 4 presents the behavior of the linearized model and the control law applied to a Navier-Stokes 3D solver. The ability of the feedback control law to reject disturbances is also discussed.

2. FLOW DESCRIPTION

Coherent structures of turbulence in plane free shear layer can be viewed in many flow visualization experiments. It was shown in Brown and Roshko (1974) and

Bernal and Roshko (1986) that turbulence is conducted by large spanwize roller vortices surrounded by smaller quasi-streamwize rib vortices. Roller vortices come from the development of perturbation due to Kelvin-Helmholtz instability leading to vortex shedding at Strouhal frequency, near the inflection point of the velocity profile, see Michalke (1965) and Monkewitz and Huerre (1982). Rib vortices come from three-dimensional shear instabilities in the thin vortical braid region between the rollers, see Corcos and Lin (1984). Together with spanwise oscillations of rollers, they speed up the transition to fully three-dimensional turbulence. Figure 1 shows an illustration of the organization of the turbulent mixing layer in the self-similar region from Carlier and Sodjavi (2016).

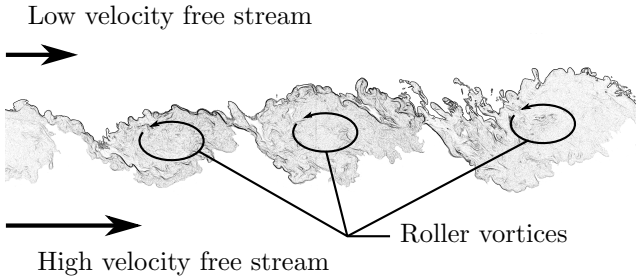

Fig. 1. Illustration of the organization of the turbulent mixing layer in the self-similar region (figure reproduced from Carlier and Sodjavi (2016)).

Self similar behavior of the mixing layer occurring downstream to the transition region is inescapable. Self similar behavior means geometric affinity of the turbulence statistic profiles and linear growth of the mixing layer thickness. Nevertheless, upstream conditions influence the mixing layer development in the transition and the self-similar regions. For example, the length of the transition region and the constant spreading rate in the self-similar region depend on velocity and density ratios between the two streams. Periodic excitations in upstream conditions also modify the structure of the flow in the mixing layer and its downstream evolution, at least in the transition region, by triggering the roller vortex shedding. This behavior corresponds to a convectively unstable and a typical noise amplifier flow, see figure 2. Note, however, that from the automatic control point of view this flow is considered as stable since at a given location the amplitude of a impulse disturbance is a decreasing function of time.

3. MODELING FOR FLOW CONTROL DESIGN

3.1 Governing equations

For an incompressible flow and Newtonian fluid, the motion of viscous fluid is described by the Navier-Stokes and the continuity equations:

$$\begin{cases} \left(\partial_t + \mathbf{u}^\top \nabla\right)\mathbf{u} = -\nabla p + \dfrac{1}{Re}\Delta\mathbf{u}, \\ \nabla^\top \mathbf{u} = 0, \end{cases} \tag{1}$$

where $\mathbf{u}$ is the velocity field vector defined as $[u \quad v \quad w]^\top$ and p the pressure, both being non-dimensionalized using

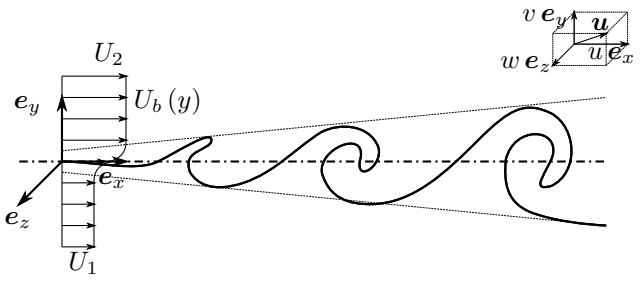

Fig. 2. Illustration of the spatially developing free shear flow. Disturbances in the shear layer (near the inflection point of the velocity profile) grow downstream. This flow is convectively unstable and a typical noise amplifier.

the velocity difference between the two free stream $U_0 = U_2 - U_1$, the volumetric mass density $\rho_0 = \rho$ and the initial thickness of the shear layer δ_0. The dynamic viscosity μ of the fluid appears in this system as a dimensionless parameter, that is the inverse of the Reynolds number $Re = \frac{\rho_0 U_0 \delta_0}{\mu}$. On this basis, all parameters, variables and values are dimensionless throughout this paper.

Let's consider $\mathbf{U}_b$ and P_b to be the steady state or the base-flow solution of system (1):

$$\begin{cases} \left(\mathbf{U}_b^\top \nabla\right)\mathbf{U}_b = -\nabla P_b + \dfrac{1}{Re}\Delta\mathbf{U}_b, \\ \nabla^\top \mathbf{U}_b = 0. \end{cases} \tag{2}$$

In this study, the Blasius solution of system (2) with free shear layer boundary conditions was approximated by:

$$\mathbf{U}_b = \begin{bmatrix} U_1 + \dfrac{1}{2}\left(\tanh(2y) + 1\right) & 0 & 0 \end{bmatrix}^\top, \tag{3}$$

where the y axis coincides with the upward transverse direction (the x axis coincides with the longitudinal streamwise direction and the z axis with the spanwise direction of the mixing layer, u, v and w are the velocity components associated with x, y and z, see figure 2).

Remark: This desired profile is homogeneous in the streamwise and spanwize directions x and z, and does not take into account the slight physical extension of the shear layer downstream.

We assumed small deviations $\mathbf{u_d} = [u_d \quad v_d \quad w_d]^\top$ and p_d around the given base-flow solution so that $\mathbf{u} = \mathbf{U}_b + \mathbf{u_d}$ and $p = P_b + p_d$. Therefore, the system (1) can be linearized and reduced to:

$$\begin{cases} \partial_t u_d + U_b\partial_x u_d + v_d\partial_y U_b = -\partial_x p_d + \frac{1}{Re}\Delta u_d, \\ \partial_t v_d + U_b\partial_x v_d = -\partial_y p_d + \frac{1}{Re}\Delta v_d, \\ \partial_t w_d + U_b\partial_x w_d = -\partial_z p_d + \frac{1}{Re}\Delta w_d, \\ \partial_x u_d + \partial_y v_d + \partial_z w_d = 0. \end{cases} \tag{4}$$

The pressure p_d is removed by using vorticity-stream function formulation, see Schmid and Henningson (2001) and McKernan (2006). Physically, isolines of stream function $\psi(x, y, t)$ at a given time are lines tangent to the flow velocity (streamlines). Using two-dimensional and incompressible flow hypothesis, the stream function is defined by:

$$U_b = +\partial_y \Psi_b, \tag{5}$$

$$u_d = +\partial_y \psi_d, \tag{6}$$

$$v_d = -\partial_x \psi_d, \tag{7}$$

and vorticity is only defined in spanwise direction z with:

$$\Omega_b = -\Delta \Psi_b, \tag{8}$$

$$\omega_d = -\Delta \psi_d. \tag{9}$$

The vorticity-stream function formulation of the linear system (4) is then given by:

$$\Delta \dot{\psi}_d = \Gamma \psi_d, \tag{10}$$

where the over-dot is used for time derivative and $\Gamma = \left[-U_b \partial_x \Delta + U_b{}'' \partial_x + \frac{1}{Re}\Delta^2\right]$ is a differential operator in which $U_b{}''(y)$ is the second derivative of $U_b(y)$. It is of note that a plane wave perturbation leads equation (10) to the well know Rayleigh or Orr-Sommerfeld equations, see Schmid and Henningson (2001).

3.2 Boundary conditions

The considered domain was assumed to be inside a box of size $L_x \times L_y$. Dirichlet boundary conditions were used at the inlet ($x = 0$), at the outlet ($x = L_x$) and at the top and bottom ($y = \pm\frac{L_y}{2}$):

- at the inlet, the stream function coincided with the control signal:
$$\psi_d(x, y, t)\,|_{x=0} = \psi_{d\,inlet}(y, t); \tag{11}$$
- at the outlet, a simplified convection equation was solved to describe the stream function boundary condition:
$$[\partial_t + (U_1 + \frac{1}{2})\partial_x]\,\psi_d|_{x=L_x} = 0; \tag{12}$$
- at the top and bottom, we imposed:
$$\psi_d(x, y, t)\,|_{y=\pm\frac{L_y}{2}} = 0. \tag{13}$$

Remark: As the difference between streamline values at any two points gives the volumetric flow rate through any curve connecting those two points, such boundary conditions impose zero value of the flow rate through the inlet boundary.

3.3 Control Design

To explicitly highlight the influence of the control signal, we converted the homogeneous equation (10) with the unhomogeneous condition (11) to an unhomogeneous equation with a homogeneous condition. To do that, the stream function is broken down into:

$$\psi_d = \psi_h + \psi_c, \tag{14}$$

where $\psi_c(x, y, t)$ describes the way the control signal acts on the flow, see Joshi et al. (1997), Joshi et al. (1999), McKernan (2006) and Tatsambon Fomena and Collewet (2011), while $\psi_h(x, y, t)$ describes the part of the stream function with homogeneous boundary conditions:

$$\begin{cases} \psi_h|_{x=0} = 0, \\ \psi_h|_{y=\pm\frac{L_y}{2}} = 0, \\ [\partial_t + (U_1 + \frac{1}{2})\partial_x]\ \psi_h|_{x=L_x} = 0. \end{cases} \tag{15}$$

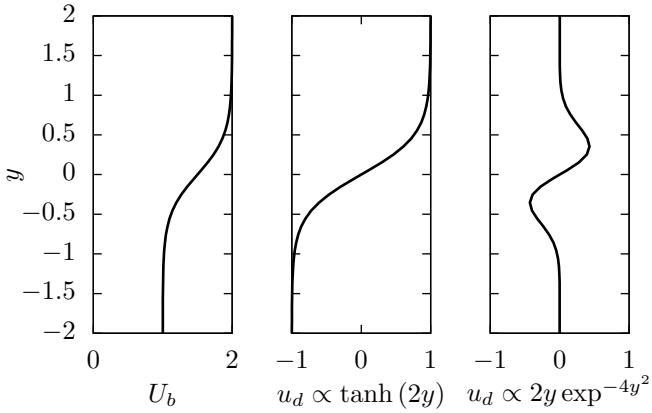

Fig. 3. Velocity profiles: Left, base-flow; Center, co-flowing stream control; Right, wall bounded jet control.

Therefore, the homogeneous equation (10) becomes:

$$\Delta \dot{\psi}_h = \Gamma \psi_h - \left(\Delta \dot{\psi}_c - \Gamma \psi_c\right). \tag{16}$$

As proposed by Joshi et al. (1997) and McKernan (2006), we also assumed that $\psi_c(x, y, t)$ can be rewritten as a separable function of space and time:

$$\psi_c(x, y, t) = f(x, y)\,\phi(t) = g(x)\,h(y)\,\phi(t), \tag{17}$$

where

- $g(x)$ describes the penetrating effect of the actuator in the streamwise direction. We considered in this paper:
$$g(x) = \exp^{-\left(\frac{x}{4}\right)^2}. \tag{18}$$
However, simulation results (not presented in this paper) showed that the form of $g(x)$ does not play an important role related to the convergence of the control law as long as $g(x)$ is a continuous and decreasing function of x.
- $h(y)$ describes the way the actuator acts at $x = 0$, that is, the way it modifies the velocity profile $u_d(y)$. We realistically modeled two kinds of actuators:
  (1) The first one is related to a co-flowing streams control generated by wind blowers:
  $$u_d(y) \propto \partial_y h(y) = \tanh(2y); \tag{19}$$
  (2) The second one is related to a wall bounded jet generated by plasma or jet actuators:
  $$u_d(y) \propto \partial_y h(y) = 2y\exp^{-4y^2}. \tag{20}$$
  Figure 3 depicts the velocity profiles of the base flow and the two types of input control.
- $\phi(t)$ is the control signal, therefore it only modifies the amplitude of $f(x, y)$ in equation (17).

Consequently, substituting (17) into equation (16), we obtained:

$$\Delta \dot{\psi}_h = \Gamma \psi_h - \left(\Delta f \dot{\phi} - f_\Gamma \phi\right), \tag{21}$$

where $f_\Gamma(x, y)$ is the result of the differential operator Γ applied to $f(x, y)$.

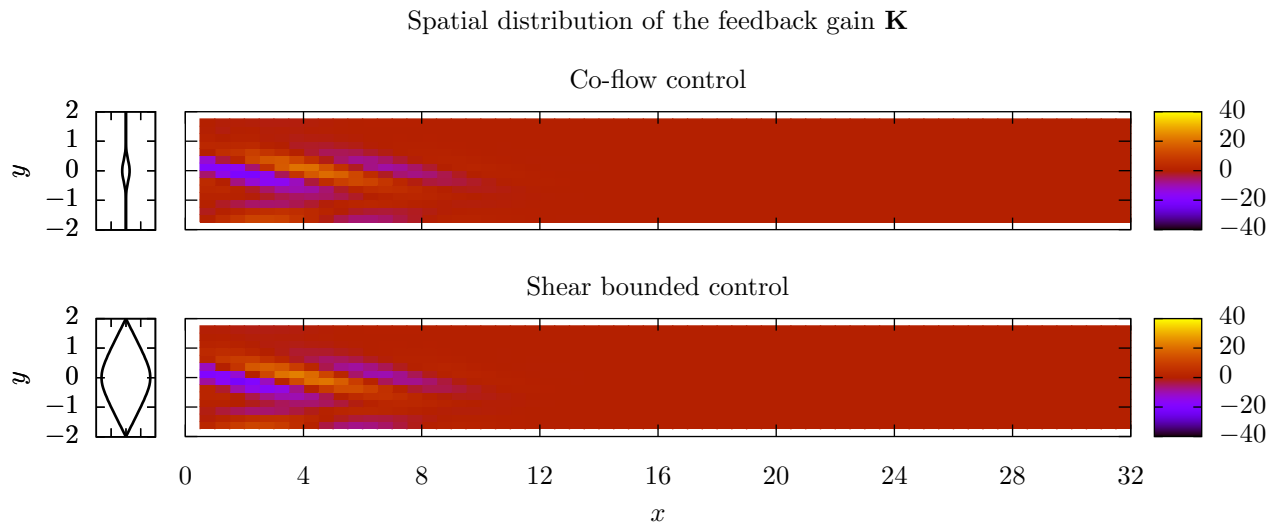

Fig. 4. Spatial distribution of the feedback gain $\mathbf{K}$.

To solve equation (21) a finite difference scheme was used. To do that, the stream function ψ_h was spatially discretized on a cartesian mesh as follows:

$$\boldsymbol{\psi}_h = \left[[\psi_{1,1} \cdots \psi_{nx,1}] \cdots [\psi_{1,ny} \cdots \psi_{nx,ny}]\right]^\top, \tag{22}$$

with $\psi_{i,j} = \psi_h(x_i, y_j)$.

More precisely, a second centered finite difference scheme was used to approximate the spatial derivative in equation (21), leading to:

$$\mathbf{L}\dot{\boldsymbol{\psi}}_h = \mathbf{G}\boldsymbol{\psi}_h - \mathbf{F}\dot{\phi} + \mathbf{F}_\Gamma\phi, \tag{23}$$

where $\boldsymbol{\psi}_h$, $\mathbf{F}$ and $\mathbf{F}_\Gamma$ were $(nx \times ny)$-dimensional vectors with $\mathbf{F} := f$ and $\mathbf{F}_\Gamma := \Gamma f$, and $\mathbf{L}$ and $\mathbf{G}$ were $(nx \times ny)$-full rank matrices with $\mathbf{L} := \Delta$ and $\mathbf{G} := \Gamma$, representing the spatial discrete operators of Δ and Γ respectively.

To recover a standard formulation of a Linear Time-Invariant (LTI) continuous-time system, we introduced as the state vector:

$$\mathbf{X} = \psi_h + \mathbf{F}\phi, \tag{24}$$

leading to

$$\dot{\mathbf{X}}(t) = \mathbf{A}\mathbf{X}(t) + \mathbf{B}\mathbf{U}(t), \tag{25}$$

where:

- $\mathbf{A} = \mathbf{L}^{-1}\mathbf{G}$ is the state or the system matrix;
- $\mathbf{B} = \mathbf{L}^{-1}(\mathbf{F}_\Gamma - \mathbf{G}\mathbf{F})$ is the input or the control matrix (column matrix in this study);
- $\mathbf{U} = [\phi]$ is called the input or the control vector (one-dimensional vector in this study).

3.4 Control law

First, let us remark that $\mathbf{X}$ (see equation 24) is nothing else than ψ_d (see equation 14) evaluated on the rectangular cartesian mesh (see definition 22). Therefore, recovering in an efficient way the state of the flow by using an image sensor is possible, see overview about flow measurements from image sequences by Heitz et al. (2010). Note that this approach of using an image sensor in the context of fluid flow closed-loop control was validated in Tatsambon Fomena and Collewet (2011) and Gautier and Aider (2014).

Since we had a model that describes the way the control signal $\mathbf{U}(t)$ acts on the flow, it was possible to derive a closed-loop control scheme. We simply proposed a Linear-Quadratic Regulator (LQR) over infinite-horizon. The cost to minimize was:

$$J = \int_0^\infty \left[\mathbf{X}^\top(t)\,\mathbf{Q}\mathbf{X}(t) + \mathbf{U}^\top(t)\,\mathbf{R}\mathbf{U}(t)\right] dt, \tag{26}$$

with $\mathbf{Q} = \mathbf{Q}^\top \geq 0$ (symmetric positive semi-definite matrix) and $\mathbf{R} = \mathbf{R}^\top > 0$ (symmetric positive definite matrix).

The matrix $\mathbf{Q}$ can be for example, an identity matrix or defined to consider the turbulent kinetic energy of the system in the cost function (see McKernan (2006)) or the enstrophy.

Therefore, the control signal was:

$$\mathbf{U}(t) = [\phi(t)] = -\mathbf{K}\mathbf{X}(t), \tag{27}$$

with $\mathbf{K} = \mathbf{R}^{-1}\mathbf{B}^\top\mathbf{P}$ and $\mathbf{P}$ the solution of the well known algebraic Riccati equation:

$$\mathbf{A}^\top\mathbf{P} + \mathbf{P}\mathbf{A} - \mathbf{P}\mathbf{B}\mathbf{R}^{-1}\mathbf{B}^\top\mathbf{P} + \mathbf{Q} = 0. \tag{28}$$

4. SIMULATION RESULTS

In this section, we first validate the linearized model derived in section 3 and then show that controling a non-linear free shear flow is possible from this linearized model.

4.1 Behavior of the linearized model

The state space model was implemented in Matlab 2012. The 2D computational domain $L_x \times L_y = 32 \times 4$ was discretized on a Cartesian grid of $nx \times ny = 65 \times 17$ mesh nodes so that $x = [0, 64]$ and $y = [-2, 2]$ with $Re = 100$. From the different choices for $\mathbf{Q}$ and $\mathbf{R}$, smaller cost value could be obtained with $\mathbf{Q} = q^2\mathbf{I}$ and $\mathbf{R} = r^2\mathbf{I}$ highly

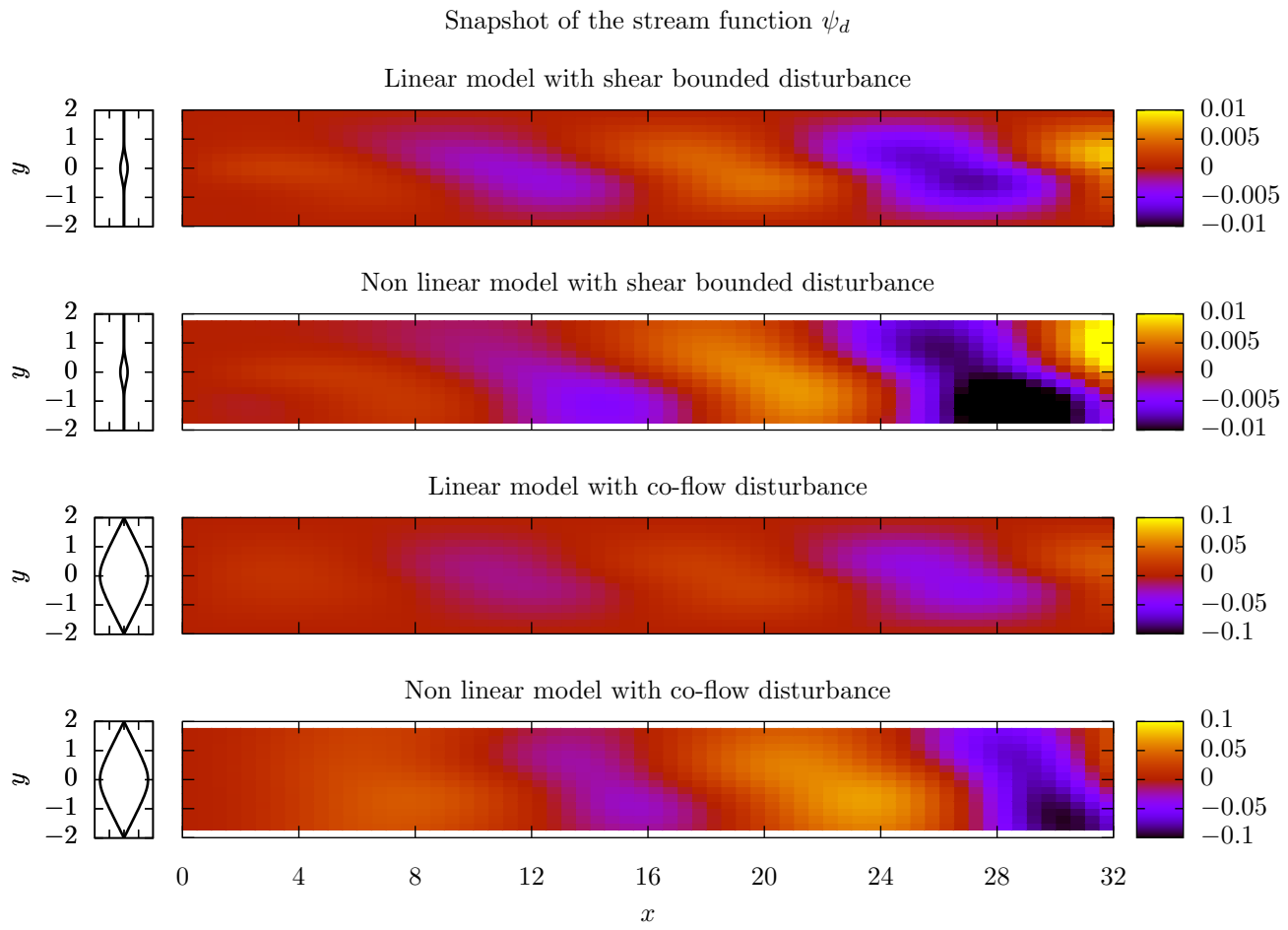

Fig. 5. Snapshots of the stream function ψ_d: Comparison between linear and non linear model for two kinds of input disturbances with sinusoidal amplitude.

depending on the ratio $\frac{r}{q}$. Results are given in this section for $q = 10$ and $r = 1$.

Numerical computation of the matrix $\mathbf{A}$ was thereafter possible. First, its eigenvalues were computed. Since they all belonged to the left half complex plane, that means that the system was stable around the desired state, as expected for convectively unstable and a typical noise amplifier flow (disturbances are amplified downstream).

Furthermore, the spatial representation of the feedback gain $\mathbf{K}$ is very interesting. Figure 4 depicts $\mathbf{K}$ for the co-flow control ($u_d(y) \propto \tanh(2y)$) and for the shear bounded control ($u_d(y) \propto 2y\exp^{-4y^2}$). The two maps are very similar. There is a discernable spatial organization that can correspond to a train of propagating Kelvin-Helmholtz vortices (while there is no *a priori* in the LQR method about the time variation of the disturbances). Amplitude of the feedback gain is decreasing downstream and in the sideways direction, so that the region of high amplitude region is limited to the proximity of the onset of the shear layer. These results agree with the idea of a control signal (see equation 27) counteracting the disturbances leading to the formation of growing Kelvin-Helmholtz vortices.

4.2 Validation of the linearized model

To validate the linearized state model, we compared its behavior with a realistic non-linear model. This model was Incompact3d, an incompressible Navier-Stokes solver released under licence GNU GPL v3. The state variables were the velocity vector and the pressure. The equations were solved on a cartesian mesh stretched in the normal direction. The spatial derivative was computed using sixth-order centered compact finite difference schemes. The time advancement was performed with an explicit third-order Adams-Bashforth scheme. The pressure was processed in the spectral space, on a staggered mesh from the velocity mesh. The divergence free condition was achieved through the use of a fractional step method and a modified wave number. More details about Incompact3d and its validation, can be found in Laizet and Lamballais (2009) and Laizet et al. (2010). The MPI implementation based on pencil domain decomposition strategy is described in Laizet and Li (2011). The 3D computational domain was $L_x \times L_y \times L_z = 256 \times 256 \times 4$. This domain was discretized on a Cartesian grid (stretched in y) of $nx \times ny \times nz = 513 \times 257 \times 8$ mesh nodes, so that the grid node in Incompact3d included the grid node in Matlab. The number of nodes in the spanwise direction was as small as possible to reduce computation time. This forced a quasi-2D flow but full 3D flow was not necessary for the purpose of this study (linear

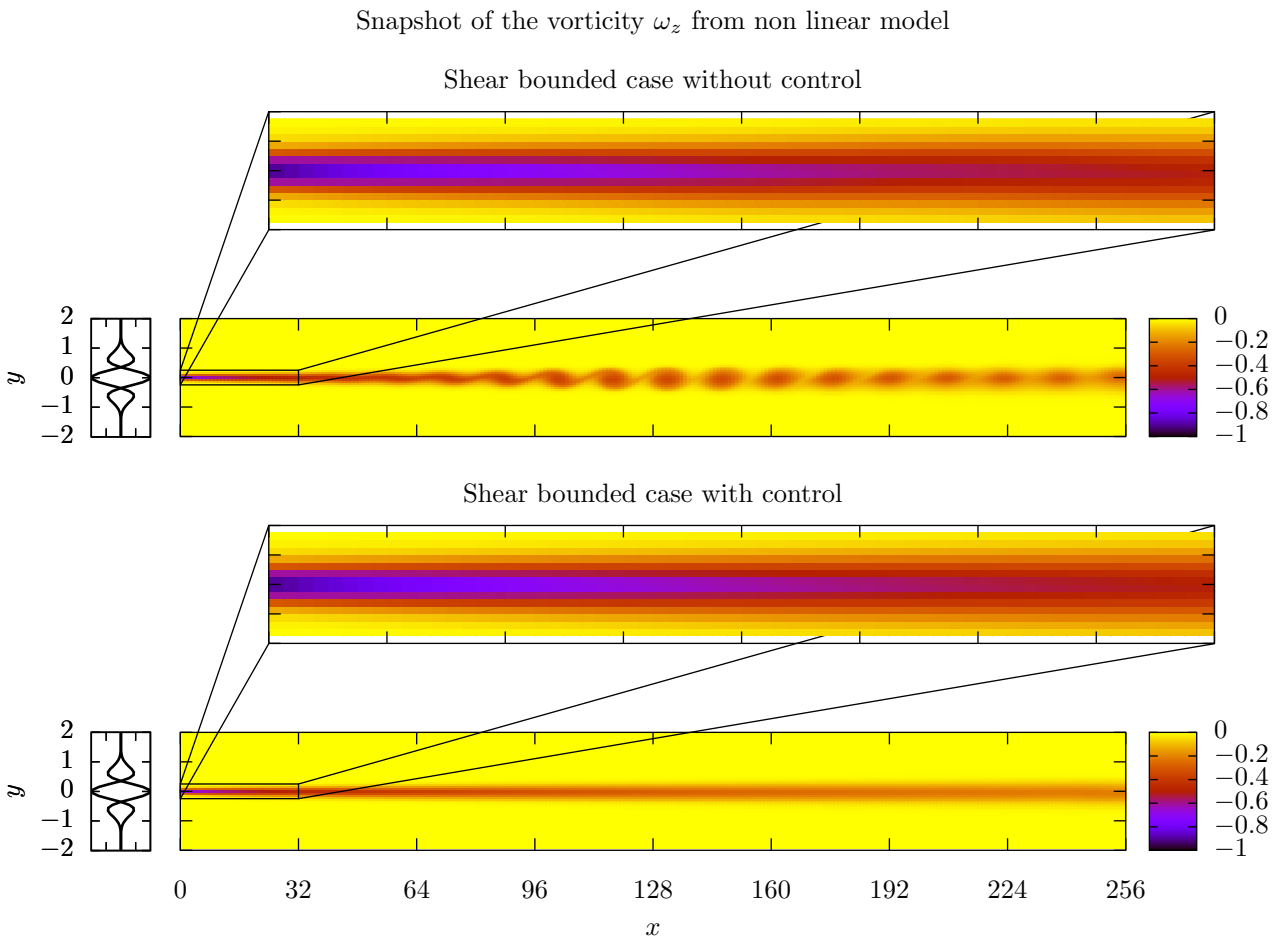

Fig. 6. Snapshots of the vorticity ω_z: Comparison with or without control in the shear bounded case.

control of non-linear flow). Same Reynolds number value of 100 was used. The control signal and the perturbation were imposed upstream using Dirichlet boundary condition. Stream function (state variable of the linear system, that have to be measured) was computed by integrating the velocity field.

To compare the behavior of both models, we considered the case where the system was forced by an input signal $\omega(t)$. The response of the linearized model was then given by the resolution of:

$$\dot{\mathbf{X}}(t) = \mathbf{A}\mathbf{X}(t) + \mathbf{B}\,\omega(t)\,. \tag{29}$$

The disturbances $\omega(t)$ was formulated as a temporal sinusoidal excitation and was given by:

$$\omega(t) = a\sin(2\pi f_{St} t)\,, \tag{30}$$

where $f_{St} = 0.1$ is approximately the Strouhal frequency (most amplified periodic perturbation, see Michalke (1965)) and $a = 0.01$ is the amplitude.

In figure 5, we present snapshots of the stream function ψ_d from simulations with the linear model (Matlab 2012) and the non linear model (Incompact3d) using co-flow and shear bounded disturbances with sinusoidal amplitude. Train of propagating Kelvin-Helmholtz vortices could be seen in both simulations, validating the representativeness of the linearized model as long as the disturbances remain sufficiently small.

4.3 Closed-loop control

The stability of the considered flow means that without sustained disturbance, the system converges to the steady solution $\mathbf{U}_b$. In this section, we look at what happens if there is periodic disturbance to the input boundary to fully validate the closed-loop control of the shear layer.

We considered that the control signal was perturbed by $\omega(t)$. Consequently, Linear Time-Invariant system (25) was rewritten as:

$$\dot{\mathbf{X}}(t) = \mathbf{A}\mathbf{X}(t) + \mathbf{B}\left[\phi(t) + \omega(t)\right], \tag{31}$$

and the feedback control law became:

$$\phi(t) = -\mathbf{K}\mathbf{X}(t) - \hat{\omega}(t)\,, \tag{32}$$

where $\hat{\omega}$ is an estimate of the disturbance ω. In this paper, we assumed that no estimation was available thus, the control law was simply $\phi(t) = -\mathbf{K}\mathbf{X}(t)$;

This signal was implemented in Incompact3d as the truth. A first run was performed to compute the steady base flow solution. This steady base flow was taken as the desired state thereafter. Then a second run continued the first one to compute a flow with fully developed disturbance. Then the control was switched On or Off in consequent runs that continued the previous one.

Figures 6 and 7 show snapshots of the vorticity ω_z a long time after the beginning of the third run in which the

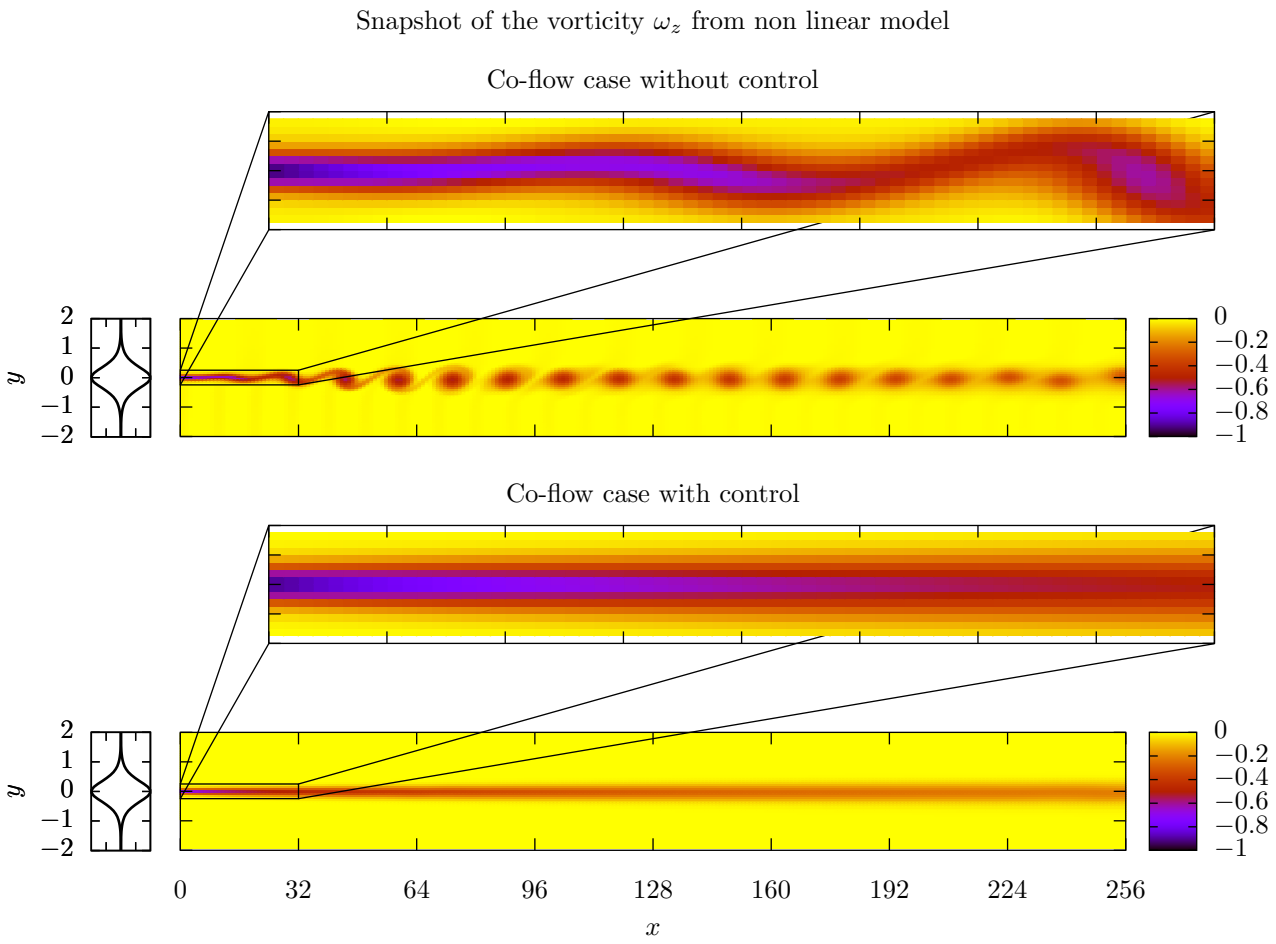

Fig. 7. Snapshots of the vorticity ω_z: Comparison with or without control in the co-flow case.

control signal was or was not applied and the control was shear bounded or in co-flow. Even if we consider that no estimation is available, those figures clearly show the benefits of using a closed-loop control. The onset of the Kelvin-Helmholtz vortices caused by the upstream disturbances was pushed further downstream so that the desired state was preserved near the input boundary, in the measured region of the state. In addition, figure 8 shows that the norm of the state vector, which is the error to the desired state, was reduced by several orders of magnitude when co-flow control and shear bounded control was applied. This performance was attained due to the control which counteracted the disturbance, as shown in figure 9.

5. CONCLUSION

In this paper, we have shown the ability of feedback control to regulate spatially developing mixing-layer flow around a steady desired state, and to reject relatively slow disturbances that matched the control. This was performed using a linear control law designed from a linearized state space model of the Navier-Stokes equations and validated on a powerful and realistic numerical Navier-Stokes 3D solver. Although LQR method is designed for stabilizing a linear system, we showed that the feedback aspects are sufficient in this study to reject disturbances, without the need of an estimate of the disturbance. Further

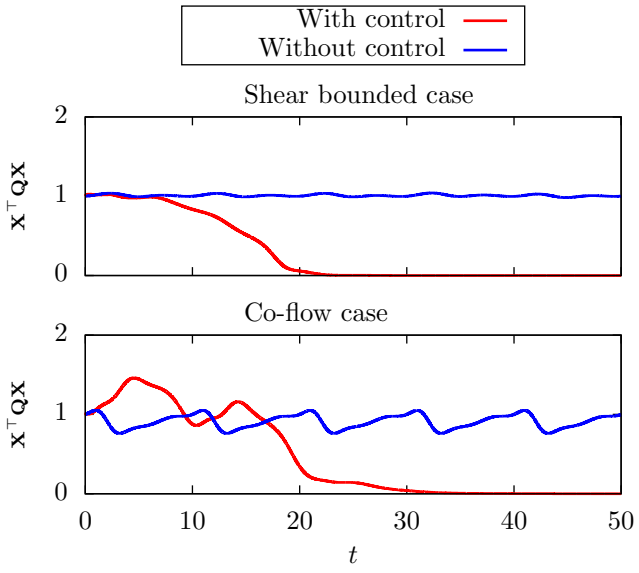

Fig. 8. Time evolution of the norm of the state vector with and without control for co-flow case (bottom) and shear bounded case (top).

works will concern the case of disturbances that does not match the control and the case of an unsteady desired state. The validation on experiments in a dedicated wind

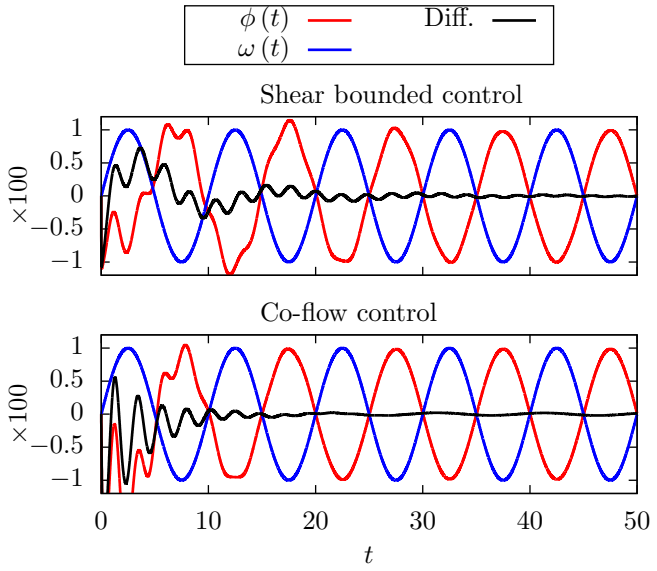

Fig. 9. Time evolution of the amplitudes of the control signal and disturbance amplitude for co-flow control (bottom) and shear bounded control (top).

tunnel, see Sodjavi and Carlier (2013) and Carlier and Sodjavi (2016), will be considered afterwards.

REFERENCES

Bernal, L.P. and Roshko, A. (1986). Streamwise vortex structure in plane mixing layers. *J. Fluid Mech.*, 170, 499–525.

Brown, G.L. and Roshko, A. (1974). On density effects and large structure in turbulent mixing layers. *J. Fluid Mech.*, 64(4), 775–816.

Brunton, S.L. and Noack, B.R. (2015). Closed-loop turbulence control: Progress and challenges. *Applied Mechanics Reviews*, 67(5), 050801–050801. doi: 10.1115/1.4031175.

Carlier, J. and Sodjavi, K. (2016). Turbulent mixing and entrainment in a stratified horizontal plane shear layer: joint velocitytemperature analysis of experimental data. *J. Fluid Mech.*, 806, 542–579. doi:10.1017/jfm.2016.592.

Corcos, G.M. and Lin, S.J. (1984). The mixing layer: deterministic models of a turbulent flow. Part 2. The origin of the three-dimensional motion. *J. Fluid Mech.*, 139, 67–95. doi:10.1017/S0022112084000264.

Gautier, N. and Aider, J.L. (2014). Feed-forward control of a perturbed backward-facing step flow. *J. Fluid Mech.*, 759, 181–196. doi:10.1017/jfm.2014.518.

Heitz, D., Mémin, E., and Schnörr, C. (2010). Variational fluid flow measurements from image sequences: synopsis and perspectives. *Experiments in Fluids*, 48(3), 369–393. doi:10.1007/s00348-009-0778-3.

Inoue, O. (1992). Double-frequency forcing on spatially growing mixing layers. *J. Fluid Mech.*, 234, 553–581. doi:10.1017/S0022112092000910.

Joshi, S.S., Speyer, J.L., and Kim, J. (1997). A systems theory approach to the feedback stabilization of infinitesimal and finite-amplitude disturbances in plane poiseuille flow. *J. Fluid Mech.*, 332, 157–184.

Joshi, S.S., Speyer, J.L., and Kim, J. (1999). Finite dimensional optimal control of poiseuille flow. *J. Guidance, Control and Dynamics*, 22(2), 340–348. doi: 10.2514/2.4383.

Kaul, U.K. (2013). *An Efficient CFD-based PID Control of Free Shear Layer Flow*. American Institute of Aeronautics and Astronautics. doi:doi:10.2514/6.2013-2986.

Kaul, U.K. (2014). *First Principles Based PID Control of Mixing Layer: Role of Inflow Perturbation Spectrum*. American Institute of Aeronautics and Astronautics. doi:doi:10.2514/6.2014-2222.

Kim, J. and Bewley, T.R. (2007). A linear systems approach to flow control. *Annu. Rev. Fluid. Mech.*, 39(1), 383–417. doi:10.1146/annurev.fluid.39.050905.110153.

Laizet, S. and Lamballais, E. (2009). High-order compact schemes for incompressible flows: A simple and efficient method with quasi-spectral accuracy. *J. Comput. Phys.*, 228(16), 5989–6015. doi: http://dx.doi.org/10.1016/j.jcp.2009.05.010.

Laizet, S., Lamballais, E., and Vassilicos, J.C. (2010). A numerical strategy to combine high-order schemes, complex geometry and parallel computing for high resolution DNS of fractal generated turbulence. *Computers & Fluids*, 39(3), 471–484. doi:http://dx.doi.org/10.1016/j.compfluid.2009.09.018.

Laizet, S. and Li, N. (2011). Incompact3d: A powerful tool to tackle turbulence problems with up to $o(10^5)$ computational cores. *International Journal for Numerical Methods in Fluids*, 67(11), 1735–1757. doi: 10.1002/fld.2480.

McKernan, J. (2006). *Control of Plane Poiseuille Flow: A theoretical and Computationnal Investigation*. Ph.D. thesis, Cranfield University, School of Engineering.

Michalke, A. (1965). On spatially growing disturbances in an inviscid shear layer. *J. Fluid Mech.*, 23, 521–544. doi:10.1017/S0022112065001520.

Monkewitz, P.A. and Huerre, P. (1982). Influence of the velocity ratio on the spatial instability of mixing layers. *Physics of Fluids*, 25(7), 1137–1143. doi: http://dx.doi.org/10.1063/1.863880.

Oster, D., Wygnanski, I., Dziomba, B., and Fiedler, H. (1978). On the effect of initial conditions on the two dimensional turbulent mixing layer. In H. Fiedler (ed.), *Structure and Mechanisms of Turbulence I*, volume 75 of *Lecture Notes in Physics*, 48–64. Springer Berlin Heidelberg.

Parezanović, V., Laurentie, J.C., Fourment, C., Delville, J., Bonnet, J.P., Spohn, A., Duriez, T., Cordier, L., Noack, B.R., Abel, M., Segond, M., Shaqarin, T., and Brunton, S.L. (2015). Mixing layer manipulation experiment. *Flow, Turbulence and Combustion*, 94(1), 155–173. doi:10.1007/s10494-014-9581-1.

Schmid, P.J. and Henningson, D.S. (2001). *Stability and transition in shear flows*, volume 142. Springer.

Sodjavi, K. and Carlier, J. (2013). Experimental study of thermal mixing layer using variable temperature hot-wire anemometry. *Experiments in Fluids*, 54(10), 1–19.

Tatsambon Fomena, R. and Collewet, C. (2011). Fluid flow control: a vision-based approach. *Int. Journal of Flow Control*, 3(2), 133–169.

Zhou, M.D. and Wygnanski, I. (2001). The response of a mixing layer formed between parallel streams to a concomitant excitation at two frequencies. *J. Fluid Mech.*, 441, 139–168. doi:10.1017/S0022112001004827.